ULTRA-NARROWBAND SELECTIVE TUNABLE FILTERS FOR VISIBLE AND INFRARED WAVELENGTH RANGES

A PREPRINT

A. D. Utyushev
Siberian Federal University, Krasnoyarsk, 660041, Russia
Siberian State University of Science and Technology, 660014, Krasnoyarsk, Russia

I. L. Isaev
Institute of Computational Modeling SB RAS, Krasnoyarsk 660036, Russia

V. S. Gerasimov
Institute of Computational Modeling SB RAS, Krasnoyarsk 660036, Russia
Siberian Federal University, Krasnoyarsk, 660041, Russia
Federal Siberian Research Clinical Center under FMBA of Russia, Krasnoyarsk, 660037, Russia

A. E. Ershov
Institute of Computational Modeling SB RAS, Krasnoyarsk 660036, Russia
Siberian Federal University, Krasnoyarsk, 660041, Russia
Federal Siberian Research Clinical Center under FMBA of Russia, Krasnoyarsk, 660037, Russia

V. I. Zakomirnyi
Siberian Federal University, Krasnoyarsk, 660041, Russia
Federal Siberian Research Clinical Center under FMBA of Russia, Krasnoyarsk, 660037, Russia
Department of Theoretical Chemistry and Biology,
School of Engineering Sciences in Chemistry, Biotechnology and Health,
Royal Institute of Technology, Stockholm, SE-10691, Sweden

I. L. Rasskazov
The Institute of Optics, University of Rochester, Rochester, NY 14627, USA

S. P. Polyutov
L.V. Kirensky Institute of Physics, Federal Research Center KSC SB RAS, 660036, Krasnoyarsk, Russia
Siberian Federal University, Krasnoyarsk, 660041, Russia
Federal Siberian Research Clinical Center under FMBA of Russia, Krasnoyarsk, 660037, Russia

H. Ågren
Federal Siberian Research Clinical Center under FMBA of Russia, Krasnoyarsk, 660037, Russia
Department of Theoretical Chemistry and Biology,
School of Engineering Sciences in Chemistry, Biotechnology and Health,
Royal Institute of Technology, Stockholm, SE-10691, Sweden

S. V. Karpov
L.V. Kirensky Institute of Physics, Federal Research Center KSC SB RAS, 660036, Krasnoyarsk, Russia
Siberian Federal University, Krasnoyarsk, 660041, Russia
Siberian State University of Science and Technology, 660014, Krasnoyarsk, Russia
Federal Siberian Research Clinical Center under FMBA of Russia, Krasnoyarsk, 660037, Russia

July 10, 2019

ABSTRACT

The interaction of non-monochromatic radiation with two types of arrays comprising both plasmonic and dielectric nanoparticles has been studied in detail. We have shown that dielectric nanoparticle arrays provide a complete selective reflection of an incident plane wave within a narrow spectral line of collective lattice resonance with a Q-factor of 10^3 or larger, whereas plasmonic refractory TiN and chemically stable Au nanoparticle arrays demonstrated high-Q resonances with moderate reflectivity. The spectral position of these resonance lines is determined by the lattice period, as well as the size, shape and material composition of the particles. Moreover, the arrays, with fixed dimensional parameters make it possible to fine-tune the position of a selected resonant spectral line by tilting the array relative to the direction of the incident radiation. These effects provide possibilities for engineering of novel selective tunable optical high-Q filters in a wide range of wavelengths: from visible to middle IR. Several highly refractive dielectric nanoparticle materials with low absorption are proposed for various spectral ranges, such as $LiNbO_3$, TiO_2, GaAs, Si, and Ge.

1 Introduction

Design and fabrication of new compact optical elements with high-Q response in the visible, near infrared (IR), and middle IR wavelength ranges is a problem in applied optics with high priority. In this regard, much attention has been focused on devices in the form of periodic one-dimensional (1D) or two-dimensional (2D) arrays composed of plasmonic or all-dielectric nanoparticles (NPs). New ideas underlying such devices have arisen from the effect first predicted in theoretical studies of regular plasmonic structures by Schatz and Markel [1, 2, 3]. According to their predictions, periodic arrays of NPs are capable to support high-Q collective lattice resonances (CLRs) in extinction spectra. CLRs occur due to the interference of fields from individual particles and the Wood-Rayleigh anomaly [4, 5]. In the general case, the Wood-Rayleigh anomaly or lattice resonance arises in periodic arrays (in particular, in diffraction gratings), in which the phase of the external field of a plane wave in the vicinity of an individual array element coincides with the phase of the field produced by neighboring elements. If this condition is satisfied within the entire array at the given wavelength, a resonance extinction occurs at this wavelength. Thus, the resonance extinction is produced by the hybrid coupling of localized low quality factor (Q-factor) resonances of NPs and their non-localized interactions covering the entire array. The position and Q-factor of these resonances depend on the geometry of the array lattice, the material composition and the shape of the NPs [6]. Under particular conditions, the Q-factor of such resonances can exceed 10^2–10^3 times the Q-factor of a single NP.

CLRs in periodic arrays of plasmonic [7, 8, 9, 10, 11, 12, 6] and all-dielectric [13, 14, 15, 16, 17, 18] NPs have been extensively discussed during the recent decade owing to the great number of potential applications in color printing [19, 20, 21, 22], biosensing [23, 24, 25, 26], lasing [27, 28], fluorescence enhancement [29] and other applications [30, 31, 6]. Highly-efficient reflective filters in the form of 1D [32, 33, 34, 35] or 2D [36, 37, 38, 39, 40] gratings which make it possible to extract required spectral lines from a non-monochromatic flux represent a most important emerging application of CLRs.

The goal of our paper is to verify the relevance of the concept of CLRs for solving applied problems and the advantages they can offer. Within the frame of this goal we propose the design of a device that makes it possible to select radiation in the reflection mode from the spectral continuum within a tunable ultra-narrow spectral line and to control its position with a high Q-factor. To achieve this goal, the following problems are solved: obtaining data on the optimal structure of the device — particle size and shape, lattice period and a particle material.

2 Methods

We consider 2D arrays of NDs with height H and radius R arranged in a regular square lattice with period h, as shown in Fig. 1(a). The arrays are embedded in a homogeneous environment with refractive index $n_m = 1.45$, which corresponds to quartz in the spectral range under study. Such structures can be fabricated using lithography technique on a quartz substrate and subsequent sputtering a layer of quartz on top of the array. A homogeneous environment is an important factor in the model, because the Q-factor of CLR drops dramatically in the case of the half-space geometry, where the substrate and the superstrate have different refractive indices [41]. The reflection spectra of such structures are calculated with commercial Finite-Difference Time-Domain (FDTD) method software [42]. FDTD is a widely used computational method of electrodynamics, which in general shows excellent agreement with experimental results for CLRs [8, 43, 11, 40]. The optical response of the infinite array is simulated by considering the single particle unit cell with periodic boundary conditions (BC) applied at the lateral boundaries of the simulation box and perfectly matched layers (PML) used on the remaining top and bottom sides, as shown in Fig. 1(b). Arrays are illuminated from
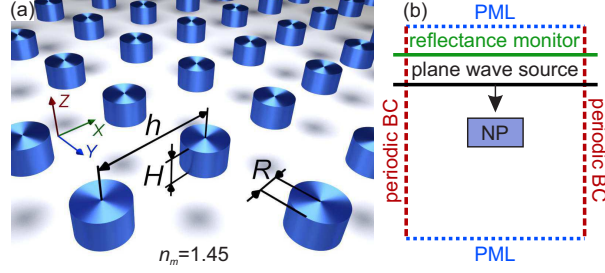
Figure 1: (a) Sketch of the ND array under consideration; (b) scheme of FDTD simulation.
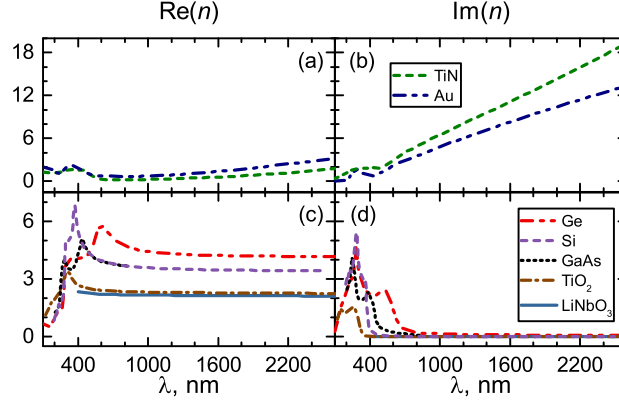

Figure 2: Real and imaginary parts of complex refractive index n for (a) and (b) plasmonic TiN [45] and Au [46]; (c) and (d) all-dielectric LiNbO$_3$ [47] (here we consider only ordinary refractive index), TiO$_2$ [48], GaAs [49], Si [50] and Ge [51].

the top by plane waves with normal incidence along the Z axis and polarization along the Y axis. The reflection has been calculated at the top of the simulation box using a discrete Fourier transform monitor which is placed above the plane-wave source. The angular dependencies were obtained using the broadband fixed angle source technique [44]. An adaptive mesh has been used to accurately reproduce the nanodisk shape. Finally, extensive convergence tests for each set of parameters have been performed to avoid undesired reflections on the PMLs.

We study arrays of both plasmonic (Au and TiN) and all-dielectric (LiNbO$_3$, Si, Ge, TiO$_2$, GaAs) nanoparticles. Figure 2 shows tabulated experimental data for the real and imaginary parts of the complex refractive index n which have been used for each material.

3   Results

The lattice period h varies in accordance with Rayleigh anomalies ($\pm$1,0) and (0,$\pm$1), the positions of which for the case of normal incidence and homogeneous environment with refractive index n_m are defined as

$$\lambda_{p,q} = hn_m/\sqrt{p^2 + q^2} \,, \tag{1}$$

where p and q are integers corresponding to the order of the anomaly. (1) describes the condition of constructive interference for particles within the XOY plane [52]. Note that λ here is the vacuum wavelength. CLRs are observed in arrays of both types: plasmonic and dielectric ones.

Before discussing CLR in NP arrays we note that the shape of the NPs is an important parameter that affects the Q-factor of the CLRs. In the calculations we examined two types of the NP shapes in the form of nanodisks and nano-parallelepipeds. Both shapes can simply be experimentally fabricated. As we found that NDs demonstrate slightly higher value of Q-factors compared to nano-parallelepipeds, the further studies were conducted with NDs only. It was found that when the disk height was equal to its radius the Q-factor was maximum.

4

3.1 Reflection spectra of plasmonic nanoparticle arrays

Plasmonic nanoparticle arrays were the first type of structures used for observation of collective lattice resonance [2, 1, 3]. Gold is a widely used material in these arrays for which surface lattice resonances are observed in the red range of the visible spectrum [7, 8, 9].

The use of TiN ND arrays (Fig 3) provides moderate reflectivity with a high Q-factor of CLRs in the telecommunication spectral range. The optimal TiN ND radius is 90 nm. A larger particle size results in a decrease of the reflectivity and the Q-factor. This suppression of surface plasmon resonances under extreme conditions [53, 54, 55] (heating of particles by pulsed laser radiation) results in a reduction of the Q-factor and CLR amplitude.

In particular, for the CLR line $\lambda = 1100$ nm in Fig 3 the Q-factor equals $1.5 \cdot 10^3$ at $T = 23°C$, $Q = 1.1 \cdot 10^3$ at $T = 400°C$, and $Q = 0.7 \cdot 10^3$ at $T = 900°C$. Thus, the high radiation resistance of TiN can be an additional advantage when using arrays exhibiting CLRs at high temperatures [12]. The use of TiN as a plasmonic material with high radiation resistance provides an extreme stability at high temperatures compared to conventional plasmonic materials (Au and Ag).
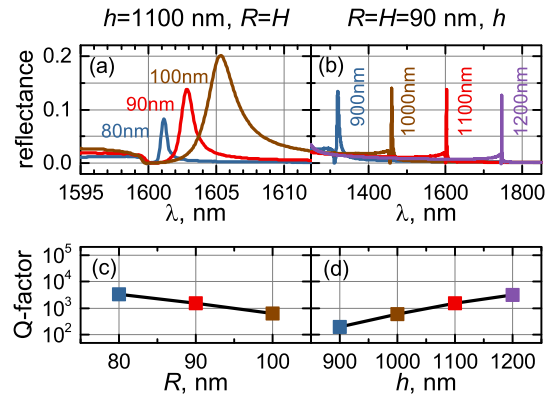

Figure 3: Reflection spectra for TiN ND arrays with: (a) fixed $h = 1100$ nm, and for different $R = H$ as shown inlegend, (b) fixed $R = H = 90$ nm and for different h as shown in legend; (c) and (d) corresponding quality factors of CLRs.

Au ND arrays (Fig 4) demonstrate CLRs in the long-wavelength part of visible and near IR ranges — away from the telecommunication range. Reflectivity and Q-factor of the Au ND array are somewhat higher compared to TiN.
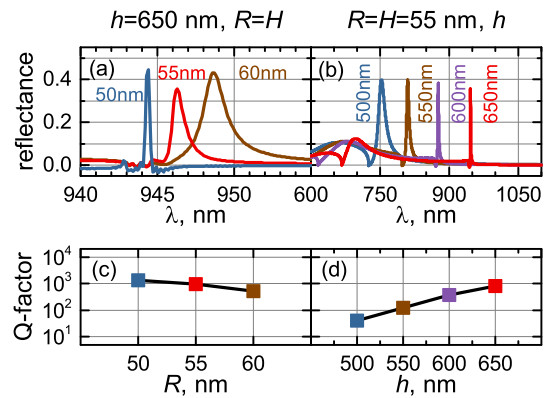

Figure 4: Reflection spectra for Au ND arrays with: (a) fixed $h = 650$ nm, and for different $R = H$ as shown in legend, (b) fixed $R = H = 55$ nm and for different h as shown in legend; (c) and (d) corresponding quality factors of CLRs.
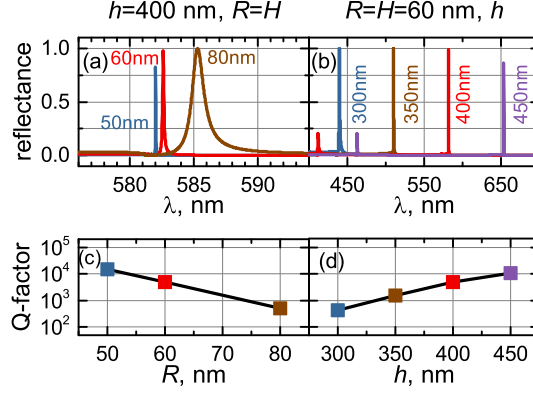
Figure 5: Reflection spectra for LiNbO$_3$ ND arrays with: (a) fixed $h = 400$ nm, and for different $R = H$ as shown in legend, (b) fixed $R = H = 60$ nm and for different h as shown in legend; (c) and (d) corresponding quality factors of CLRs.

Figure 6: Reflection spectra for TiO$_2$ ND arrays with: (a) fixed $h = 400$ nm, and for different $R = H$ as shown in legend, (b) fixed $R = H = 50$ nm and for different h as shown in legend; (c) and (d) corresponding quality factors of CLRs.
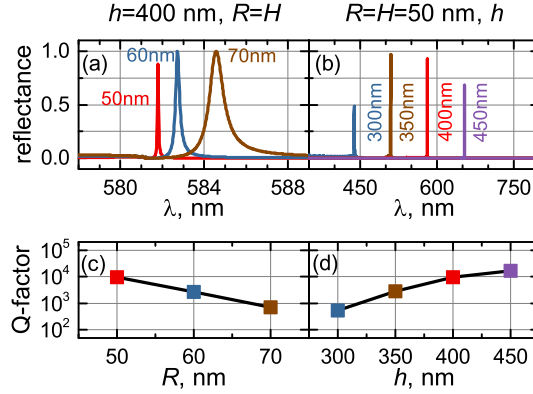
3.2 Dielectric nanoparticle arrays

3.2.1 Reflection spectra

In the case of dielectric structures the main requirements imposed on the type of employed NP materials are combination of high real part of the refractive index $\mathrm{Re}(n)$ and a low imaginary part $\mathrm{Im}(n)$ for different spectral ranges which ensures low absorption inside the particles. Figs 2(c),(d) show, in particular, the refractive indices of the following suitable lossless materials satisfying these requirements: LiNbO$_3$, TiO$_2$, Si, GaAs, Ge. In this paper we have selected materials for each spectral range to obtain high-Q CLR in each given case.

Two materials were chosen for the visible range: LiNbO$_3$ and TiO$_2$. Figures 5(a),(b) and 6(a),(b) with reflection spectra of LiNbO$_3$ and TiO$_2$ ND arrays show that the larger the particle size, the lower the Q-factor, but at the same time the higher the reflection coefficient. So the optimal combination of these factor gives a particle radius of 60 nm with a Q-factor equal to 10^3. Figures 5(c),(d) show that employing this material in ND arrays provides ultra-narrowband resonances in the entire visible range with a Q-factor over 10^3 and high reflection. The utilization of TiO$_2$ in ND arrays also provides high reflectivity and Q-factor, however, with smaller size of the particle — 50 nm compared to LiNbO$_3$ that results in narrowing the spectral range with high reflectivity (Fig. 6). The next step is to vary the lattice period with the given optimal radius. Calculations show that the Q-factor of the CLR increases with wavelength. Additional opportunities to increase the CLR Q-factor are opened by changing the size and shape of the particles, as well as the optical properties of their material.
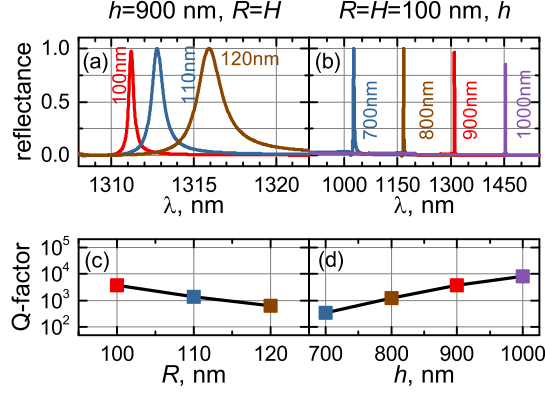
Figure 7: Reflection spectra for Si ND arrays with: (a) fixed $h = 900$ nm, and for different $R = H$ as shown in legend, (b) fixed $R = H = 100$ nm and for different h as shown in legend; (c) and (d) corresponding quality factors of CLRs.
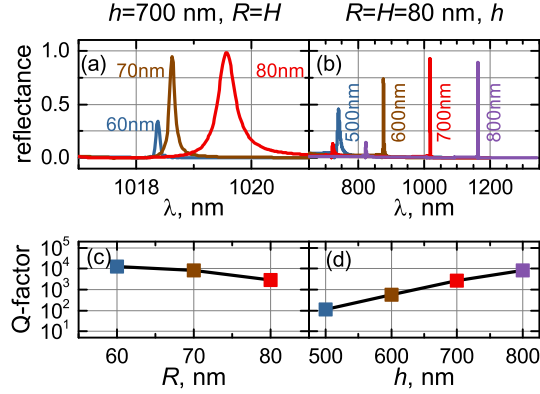

Figure 8: Reflection spectra for GaAs ND arrays with: (a) fixed $h = 700$ nm, and for different $R = H$ as shown in legend, (b) fixed $R = H = 80$ nm and for different h as shown in legend; (c) and (d) corresponding quality factors of CLRs.

The best materials for the near-IR range are Si and GaAs. These materials in the IR range demonstrate the properties of a dielectric (Fig. 2) with a near-zero imaginary part of the refractive index and its high real part, which makes it possible to excite Mie resonances in such particles [56] with radius below 100 nm — much smaller than the wavelength. Fig. 7 shows the reflection spectra of Si ND arrays with ND radii $R = 100$, 110, and 120 nm and radius/height ration $R/H = 1$. Besides that, Figure 7 shows that CLRs with appear reflected radiation in the entire telecommunication wavelength range by varying the array period. Reflection spectra for GaAs ND arrays have optimal characteristics in the range between visible and telecom wavelengths (Fig. 8). The optimal ND radius equals 70 nm and period 600–700 nm with ultrahigh Q-factor.

The use of the Ge ND arrays provides high reflectivity and Q-factor in the middle IR range with optimal ND radius 165 nm. A smaller size of the particle results in a decrease of reflectivity, larger ones are accompanied by lower Q-factors (Fig. 9).

It can be seen from Figs 5(a)–9(a) that, generally, the increase in the ND radius while maintaining the height H is accompanied by a long-wavelength shift of the CLR and a decrease of the Q-factor. The reflection coefficient is slightly growing towards longer wavelengths (Fig. 5–9) with a subsequent fall. It is found that an increase of ND height with fixed ratio R/H, results in a long-wavelength shift of the resonance and decrease of both the Q-factor and the reflection coefficient. The increase of the lattice period with preservation of the ratio R/H, is accompanied by a long-wavelength shift of CLR, a non-monotonic increase of the Q-factor, and by the decrease of the reflection coefficient.
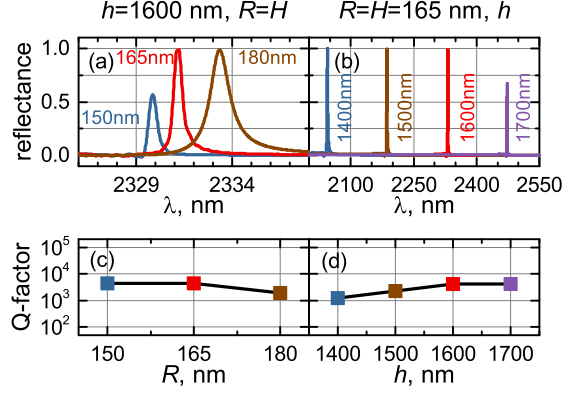
7

Figure 9: Reflection spectra for Ge ND arrays with: (a) fixed $h = 1600$ nm, and for different $R = H$ as shown in legend, (b) fixed $R = H = 165$ nm and for different h as shown in legend; (c) and (d) corresponding quality factors of CLRs.
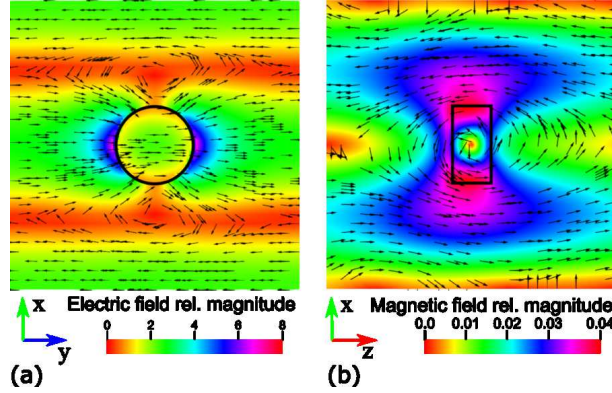

Figure 10: (a) Electric and (b) magnetic field distribution in XOY and XOZ planes. Si ND with $R = H = 120$ nm and array period $h = 900$ nm at maximum reflection wavelength $\lambda = 1317$ nm. Polarization direction along the Y axis. Solid black line outlines the ND's boundaries.

3.2.2 Electromagnetic field configuration

The study of the radiation reflection from nanoparticle arrays calls for a clarification of what type of resonance excitation is associated with a high generated reflection. Fig. 10(a),(b) show the configuration of electric and magnetic fields in orthogonal planes inside the unit cell of Si ND with $R = H = 120$ nm and array period $h = 900$ nm at the maximum reflection wavelength $\lambda = 1317$ nm (see the spectrum in Fig. 7(a). Fig. 10(a) shows the spatial profile of the electric field calculated in a plane of the array, while Fig. 10(b) shows the spatial profile of the magnetic field in the plane orthogonal to both the radiation incidence plane and the array plane. As can be seen, this configuration of the electromagnetic field coincides with the classical pattern of an oscillating electric dipole.

3.2.3 Dimensional invariance of collective lattice resonances

Arrays of all-dielectric NPs demonstrate an important feature in conditions of utilizing materials with zero dispersion. In particular, the spectral position of collective lattice resonance in TiO_2 NP arrays as all-dielectric systems can be predicted by multiplying all dimensional parameters of the array (particle radius, height and lattice period) by the same number K. The new resonance position will correspond to $K\lambda_r$ (where λ_r is the previous wavelength value (Fig. 11). This feature is a consequence of the scale-invariance of Maxwell's equations in the case of non-absorbing and non-dispersive materials. This is the easiest way to predict reflection at a specific wavelength. So if we determine the optimal parameters of the structure (with maximum reflectivity and the CLR Q-factor) by applying the multiplier K to all lattice parameters we can predict the resonance position at any required wavelength. Fig. 11(a),(b) show a twofold (for TiO_2 ND array) and one and a half (for Si ND array) increase in the parameters of the arrays with corresponding
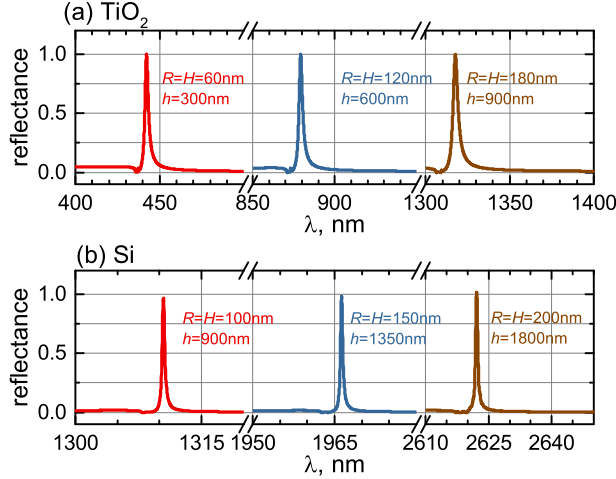
8

Figure 11: Reflection spectra for (a) Si and (b) TiO$_2$ ND arrays with different sizes but with fixed R/H and P/R ratios.
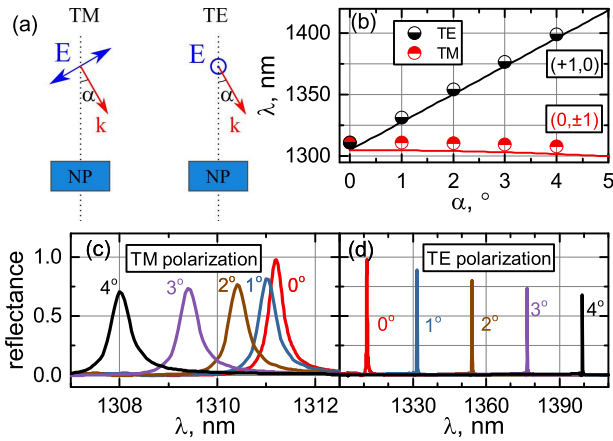

Figure 12: (a) Sketch of the vector configuration for TM and TE polarization, (b) spectral positions of (+1,0) and (0,±1) Wood-Rayleigh anomalies as a functions of the incidence angle (solid lines) and corresponding positions of reflectance maxima (partially filled circles); Incidence angle dependence of the reflection spectra for Si ND array with $h = 900$ nm and $R = H = 100$ nm for (c) TM and (d) TE polarizations.

shift of the resonance lines, something that demonstrates the scale invariance of CLRs. Scale invariance allows to design and to fabricate optical filters for operation in an arbitrary spectral range from near to far IR.

3.3 Fine tuning the resonance line using the angular dependence of reflection

The possibility of employing NP arrays for spectral selection of radiation with required wavelength in the reflection mode requires the possibility to deflect the selected monochromatic radiation away from the incidence direction of the non-monochromatic radiation by tilting the array at least a few degrees. The results from investigating this possibility are shown in Fig. 12. It is found that the slope of the array in the range of $\alpha = 1° - 4°$ is accompanied by a slight decrease in Q-factor of resonance and reflection coefficient. However, the more important effect of this tilting is the shift of the resonance line to the short-wavelength range by about 3 nm in one plane, and to the long-wavelength range by over 100 nm — in another plane. Obviously, the found property of arrays makes it possible to use them for spectral selection and to fine-tune the spectral position of the resonance line to the required wavelength.

9

Our calculations show that at larger angles ($\alpha > 4°$), the resonance shift continues to grow. However, with the increase in the angle up to $\alpha > 20°$ the resonance line acquires short-wavelength spectral satellites with growing amplitude, which along with a decrease of the Q-factor impair the selectivity of filtration. To prevent such effects, one should limit the angle to 8–10° or less. Similar results have been obtained for other materials.

Figs. 12(c),(d) demonstrate a decrease of the CLR Q-factor from $Q = 3.6 \cdot 10^3$ for $\alpha = 0°$ to $Q = 2.9 \cdot 10^3$ and $Q = 10^3$ for $\alpha = 4°$ for TM and TE polarizations, respectively. Fig. 12 also demonstrates different effects of tilting the array around Y axis for different polarization of incident radiation. Rotations of the array around the Y axis for TE polarization turn up to be more sensitive to positions of the CLRs than for TM polarization. The explanation of this feature is given as follows. The position of the Wood-Rayleigh anomaly in this case follows simple rules. The condition for constructive interference for the case of oblique incidence and square unit cell (the wave vector is in XOZ plane) reads as

$$k_x h = 2\pi p + kh \sin \alpha, \quad k_y h = 2\pi q \ . \tag{2}$$

Here k_x, k_y are x and y components of the scattered wave vector, p and q are integers which represent the the phase difference (in 2π units) between waves scattered by two adjacent elements of the array and incident wave in the x and y directions, α is the angle between the wave vector of the incident wave and the Z axis, and k is the absolute value of the wave vector of the incident wave:

$$k = \frac{2\pi n_m}{\lambda} = \sqrt{k_x^2 + k_y^2} \ . \tag{3}$$

For the case of $p = 0$, which corresponds to the TM polarization, we have:

$$\lambda = \pm \frac{n_m \cos \alpha}{q} h \ . \tag{4}$$

For $q = 0$, which corresponds to the TE polarization:

$$\lambda = \frac{n_m (1 \pm \sin \alpha)}{\pm p} h \ . \tag{5}$$

Thus, the angular dependence of the spectral shift for the TM polarization obeys (4), but for TE polarization it is described by (5). These fast and slow dependencies are shown in Fig. 12(d) and do fully correspond to the spectral features in Fig. 12(a),(b).

4   Conclusion

Based on the obtained results we can make the following statements.

Periodic structures consisting of dielectric highly refractive nanoparticles with low absorption demonstrating collective lattice resonances can be used in the reflection mode as selective ultra-narrowband spectral filters. The position of spectral lines can be adjusted using the lattice period. We have found that arrays with nanoparticles of various shapes (nanodisks and nano-parallelepipeds) demonstrate similar optical properties and can be synthesized by different available experimental techniques.

Dielectric nanoparticle arrays are preferable structures for lossless narrowband reflection compared to plasmonic ones with low refraction and significant absorption of highly conductive materials in the range of the collective lattice resonances (Fig.2). Herewith minor array defects, that may occur during experimental fabrication of the structure, do not significantly affect the Q-factor of the CLRs [57].

Arrays of plasmonic nanoparticles, on the other hand, allow one to achieve a high-Q CLR response in conditions of strong NP heating (TiN), chemically aggressive media or biological environment (Au, TiN) in spite of a lower value of the reflection coefficient. The results obtained enable determining the most suitable material, both taking into account its optical characteristics and operating conditions.

Scale invariance of such arrays makes it possible to design and to fabricate filters for operation in arbitrary spectral ranges with low dispersion materials from near to far IR.

The nanoparticle arrays in the reflection mode demonstrate an optical filtering effect with fine tuning of the spectral position of the resonance line to the required wavelength by means of tilting the array toward the incident radiation.

The proposed model provides a quantitative interpretation of the angular dependence of the characteristics of a collective lattice resonance for different geometry of the radiation incidence onto array.

5   Funding Information

References

[1] Shengli Zou, Nicolas Janel, and George C. Schatz. Silver nanoparticle array structures that produce remarkably narrow plasmon lineshapes. *Journal of Chemical Physics*, 120(23):10871–10875, 2004.

[2] Shengli Zou and George C. Schatz. Narrow plasmonic/photonic extinction and scattering line shapes for one and two dimensional silver nanoparticle arrays. *Journal of Chemical Physics*, 121(24):12606–12612, 2004.

[3] Vadim A. Markel. Divergence of dipole sums and the nature of non-Lorentzian exponentially narrow resonances in one-dimensional periodic arrays of nanospheres. *Journal of Physics B: Atomic, Molecular and Optical Physics*, 38(7):L115–L121, 2005.

[4] R W Wood. On a remarkable case of uneven distribution of light in a diffraction grating spectrum. *Proceedings of the Physical Society of London*, 18(1):269–275, 6 1902.

[5] L. Rayleigh. On the dynamical theory of gratings. *Proceedings of the Royal Society A: Mathematical, Physical and Engineering Sciences*, 79(532):399–416, 8 1907.

[6] V. G. Kravets, A. V. Kabashin, W. L. Barnes, and A. N. Grigorenko. Plasmonic surface lattice resonances: a review of properties and applications. *Chemical Reviews*, 118(12):5912–5951, 6 2018.

[7] Baptiste Auguié and William L Barnes. Collective resonances in gold nanoparticle arrays. *Physical Review Letters*, 101(14):143902, 9 2008.

[8] Yizhuo Chu, Ethan Schonbrun, Tian Yang, and Kenneth B. Crozier. Experimental observation of narrow surface plasmon resonances in gold nanoparticle arrays. *Applied Physics Letters*, 93(18):181108, 11 2008.

[9] V. G. Kravets, F. Schedin, and A. N. Grigorenko. Extremely narrow plasmon resonances based on diffraction coupling of localized plasmons in arrays of metallic nanoparticles. *Physical Review Letters*, 101(8):087403, 8 2008.

[10] Michael B. Ross, Chad A. Mirkin, and George C. Schatz. Optical properties of one-, two-, and three-dimensional arrays of plasmonic nanostructures. *The Journal of Physical Chemistry C*, 120(2):816–830, 1 2016.

[11] Dmitry Khlopin, Frédéric Laux, William P. Wardley, Jérôme Martin, Gregory A. Wurtz, Jérôme Plain, Nicolas Bonod, Anatoly V. Zayats, Wayne Dickson, and Davy Gérard. Lattice modes and plasmonic linewidth engineering in gold and aluminum nanoparticle arrays. *Journal of the Optical Society of America B*, 34(3):691–700, 3 2017.

[12] Vadim I. Zakomirnyi, Ilia L. Rasskazov, Valeriy S. Gerasimov, Alexander E. Ershov, Sergey P. Polyutov, and Sergei V. Karpov. Refractory titanium nitride two-dimensional structures with extremely narrow surface lattice resonances at telecommunication wavelengths. *Applied Physics Letters*, 111(12):123107, 9 2017.

[13] Saman Jahani and Zubin Jacob. All-dielectric metamaterials. *Nature Nanotechnology*, 11(1):23–36, 1 2016.

[14] Sheng Liu, Michael B. Sinclair, Thomas S. Mahony, Young Chul Jun, Salvatore Campione, James Ginn, Daniel A. Bender, Joel R. Wendt, Jon F. Ihlefeld, Paul G. Clem, Jeremy B. Wright, and Igal Brener. Optical magnetic mirrors without metals. *Optica*, 1(4):250–256, 10 2014.

[15] Sheng Liu, Michael B. Sinclair, Sina Saravi, Gordon A. Keeler, Yuanmu Yang, John Reno, Gregory M. Peake, Frank Setzpfandt, Isabelle Staude, Thomas Pertsch, and Igal Brener. Resonantly enhanced second-harmonic generation using III–V semiconductor all-dielectric metasurfaces. *Nano Letters*, 16(9):5426–5432, 9 2016.

[16] Sheng Liu, Gordon A. Keeler, John L. Reno, Michael B. Sinclair, and Igal Brener. III-V Semiconductor nanoresonators-a new strategy for passive, active, and nonlinear all-dielectric metamaterials. *Advanced Optical Materials*, 4(10):1457–1462, 10 2016.

[17] Sheng Liu, Polina P. Vabishchevich, Aleksandr Vaskin, John L. Reno, Gordon A. Keeler, Michael B. Sinclair, Isabelle Staude, and Igal Brener. An all-dielectric metasurface as a broadband optical frequency mixer. *Nature Communications*, 9(1):2507, 12 2018.

[18] Xiaowei Wang, Leonard C. Kogos, and Roberto Paiella. Giant distributed optical-field enhancements from Mie-resonant lattice surface modes in dielectric metasurfaces. *OSA Continuum*, 2(1):32–42, 1 2019.

[19] Hyunsung Park and Kenneth B. Crozier. Multispectral imaging with vertical silicon nanowires. *Scientific Reports*, 3(1):2460, 12 2013.

[20] Julien Proust, Frédéric Bedu, Bruno Gallas, Igor Ozerov, and Nicolas Bonod. All-dielectric colored metasurfaces with silicon Mie resonators. *ACS Nano*, 10(8):7761–7767, 8 2016.

[21] Zhaogang Dong, Jinfa Ho, Ye Feng Yu, Yuan Hsing Fu, Ramón Paniagua-Dominguez, Sihao Wang, Arseniy I. Kuznetsov, and Joel K. W. Yang. Printing beyond sRGB color gamut by mimicking silicon nanostructures in free-space. *Nano Letters*, 17(12):7620–7628, 12 2017.

[22] Shang Sun, Zhenxing Zhou, Chen Zhang, Yisheng Gao, Zonghui Duan, Shumin Xiao, and Qinghai Song. All-dielectric full-color printing with TiO2 metasurfaces. *ACS Nano*, 11(5):4445–4452, 5 2017.

[23] Stefan Enoch, Romain Quidant, and Goncal Badenes. Optical sensing based on plasmon coupling in nanoparticle arrays. *Optics Express*, 12(15):3422, 2004.

[24] Ronen Adato, Ahmet A Yanik, Jason J Amsden, David L Kaplan, Fiorenzo G Omenetto, Mi K Hong, Shyamsunder Erramilli, and Hatice Altug. Ultra-sensitive vibrational spectroscopy of protein monolayers with plasmonic nanoantenna arrays. *Proceedings of the National Academy of Sciences*, 106(46):19227–19232, 11 2009.

[25] V G Kravets, F Schedin, A. V. Kabashin, and A. N. Grigorenko. Sensitivity of collective plasmon modes of gold nanoresonators to local environment. *Optics Letters*, 35(7):956, 4 2010.

[26] Nicolò Bontempi, Katie E. Chong, Henry W. Orton, Isabelle Staude, Duk-Yong Choi, Ivano Alessandri, Yuri S. Kivshar, and Dragomir N. Neshev. Highly sensitive biosensors based on all-dielectric nanoresonators. *Nanoscale*, 9(15):4972–4980, 2017.

[27] Wei Zhou, Montacer Dridi, Jae Yong Suh, Chul Hoon Kim, Dick T Co, Michael R Wasielewski, George C Schatz, and Teri W Odom. Lasing action in strongly coupled plasmonic nanocavity arrays. *Nature Nanotechnology*, 8(7):506–511, 6 2013.

[28] Son Tung Ha, Yuan Hsing Fu, Naresh Kumar Emani, Zhenying Pan, Reuben M. Bakker, Ramón Paniagua-Domínguez, and Arseniy I. Kuznetsov. Directional lasing in resonant semiconductor nanoantenna arrays. *Nature Nanotechnology*, 13(11):1042–1047, 11 2018.

[29] G Vecchi, V Giannini, and J. Gómez Rivas. Shaping the Fluorescent Emission by Lattice Resonances in Plasmonic Crystals of Nanoantennas. *Physical Review Letters*, 102(14):146807, 4 2009.

[30] Bharath Bangalore Rajeeva, Linhan Lin, and Yuebing Zheng. Design and applications of lattice plasmon resonances. *Nano Research*, 11(9):4423–4440, 9 2018.

[31] Weijia Wang, Mohammad Ramezani, Aaro I. Väkeväinen, Päivi Törmä, Jaime Gómez Rivas, and Teri W. Odom. The rich photonic world of plasmonic nanoparticle arrays. *Materials Today*, 21(3):303–314, 4 2018.

[32] Anil K. Kodali, Matthew Schulmerich, Jason Ip, Gary Yen, Brian T. Cunningham, and Rohit Bhargava. Narrowband Midinfrared Reflectance Filters Using Guided Mode Resonance. *Analytical Chemistry*, 82(13):5697–5706, 7 2010.

[33] Jui-Nung Liu, Matthew V. Schulmerich, Rohit Bhargava, and Brian T. Cunningham. Optimally designed narrowband guided-mode resonance reflectance filters for mid-infrared spectroscopy. *Optics Express*, 19(24):24182, 11 2011.

[34] Jui-Nung Liu, Matthew V Schulmerich, Rohit Bhargava, and Brian T Cunningham. Sculpting narrowband Fano resonances inherent in the large-area mid-infrared photonic crystal microresonators for spectroscopic imaging. *Optics Express*, 22(15):18142, 7 2014.

[35] Daniel B. Mazulquim, Kyu Jin Lee, Jae Woong Yoon, Leone V. Muniz, Ben-Hur V. Borges, Luiz G. Neto, and Robert Magnusson. Efficient band-pass color filters enabled by resonant modes and plasmons near the Rayleigh anomaly. *Optics Express*, 22(25):30843, 12 2014.

[36] D W Peters, R R Boye, J R Wendt, R A Kellogg, S A Kemme, T R Carter, and S Samora. Demonstration of polarization-independent resonant subwavelength grating filter arrays. *Optics Letters*, 35(19):3201, 10 2010.

[37] Fei Shen, Qianlong Kang, Jingjing Wang, Kai Guo, Qingfeng Zhou, and Zhongyi Guo. Dielectric Metasurface-Based High-Efficiency Mid-Infrared Optical Filter. *Nanomaterials*, 8(11):938, 11 2018.

[38] Jeremy Upham, Boshen Gao, Liam O'Faolain, Zhimin Shi, Sebastian A. Schulz, and Robert W. Boyd. Realization of a flat-band superprism on-chip from parallelogram lattice photonic crystals. *Optics Letters*, 43(20):4981, 10 2018.

[39] Ziyi Wang, Rongjun Zhang, and Junpeng Guo. Quadrupole mode plasmon resonance enabled subwavelength metal-dielectric grating optical reflection filters. *Optics Express*, 26(1):496, 1 2018.

[40] Ryan C Ng, Juan C Garcia, Julia R Greer, and Katherine T Fountaine. Polarization-independent, narrowband, near-IR spectral filters via guided mode resonances in ultrathin a-Si nanopillar arrays. *ACS Photonics*, 6(2):265–271, 2 2019.

[41] Baptiste Auguié, Xesús M. Bendaña, William L. Barnes, and F. Javier García de Abajo. Diffractive arrays of gold nanoparticles near an interface: Critical role of the substrate. *Physical Review B*, 82(15):155447, 10 2010.

[42] Lumerical Solutions, "FDTD Solutions".

[43] Benjamin D Thackray, Philip A Thomas, Gregory H Auton, Francisco J Rodriguez, Owen P Marshall, Vasyl G Kravets, and Alexander N Grigorenko. Super-narrow, extremely high quality collective plasmon resonances at telecom wavelengths and their application in a hybrid graphene-plasmonic modulator. *Nano Letters*, 15(5):3519–3523, 5 2015.

[44] Bin Liang, Ming Bai, Hui Ma, Naiming Ou, and Jungang Miao. Wideband analysis of periodic structures at oblique incidence by material independent FDTD algorithm. *IEEE Transactions on Antennas and Propagation*, 62(1):354–360, 1 2014.

[45] Harsha Reddy, Urcan Guler, Zhaxylyk Kudyshev, Alexander V. Kildishev, Vladimir M. Shalaev, and Alexandra Boltasseva. Temperature-dependent optical properties of plasmonic titanium nitride thin films. *ACS Photonics*, 4(6):1413–1420, 6 2017.

[46] P. B. Johnson and R. W. Christy. Optical constants of the noble metals. *Physical Review B*, 6(12):4370–4379, 12 1972.

[47] David E. Zelmon, David L. Small, and Dieter Jundt. Infrared corrected Sellmeier coefficients for congruently grown lithium niobate and 5 mol% magnesium oxide –doped lithium niobate. *Journal of the Optical Society of America B*, 14(12):3319–3322, 12 1997.

[48] J. R. DeVore. Refractive indices of rutile and sphalerite. *Journal of the Optical Society of America*, 41(6):416–419, 6 1951.

[49] D. E. Aspnes, S. M. Kelso, R. A. Logan, and R. Bhat. Optical properties of Al x Ga 1- x As. *Journal of Applied Physics*, 60(2):754–767, 7 1986.

[50] David F. Edwards. Silicon (Si). In *Handbook of Optical Constants of Solids*, pages 547–569. Elsevier, 1997.

[51] Roy F. Potter. Germanium (Ge). In *Handbook of Optical Constants of Solids*, pages 465–478. Elsevier, 1997.

[52] Nicolas Bonod and Jérôme Neauport. Diffraction gratings: from principles to applications in high-intensity lasers. *Advances in Optics and Photonics*, 8(1):156–199, 3 2016.

[53] V S Gerasimov, A E Ershov, A P Gavrilyuk, S V Karpov, H Ågren, and S P Polyutov. Suppression of surface plasmon resonance in Au nanoparticles upon transition to the liquid state. *Optics Express*, 24(23):26851, 11 2016.

[54] A E Ershov, V. S. Gerasimov, A. P. Gavrilyuk, and S. V. Karpov. Surface plasmon resonances in liquid metal nanoparticles. *Applied Physics B*, 123(6):182, 6 2017.

[55] V. S. Gerasimov, A. E. Ershov, S. V. Karpov, A. P. Gavrilyuk, V. I. Zakomirnyi, I. L. Rasskazov, H. Ågren, and S. P. Polyutov. Thermal effects in systems of colloidal plasmonic nanoparticles in high-intensity pulsed laser fields [Invited]. *Optical Materials Express*, 7(2):555–568, 2 2017.

[56] Craig F. Bohren and Donald R. Huffman. *Absorption and Scattering of Light by Small Particles*. Wiley-VCH Verlag GmbH, Weinheim, Germany, 4 1998.

[57] Vadim I. Zakomirnyi, Sergei V. Karpov, Hans Ågren, and Ilia L. Rasskazov. Collective lattice resonances in disordered and quasi-random all-dielectric metasurfaces. *Journal of the Optical Society of America B*, 36(7):E21–E29, 7 2019.